Cell. Mol. Biol. (ISSN: 1165-158X)

Journal Homepage: www.cellmolbiol.org

Cellular and Molecular Biology

Original Article

Chelerythrine induces apoptosis and ferroptosis through Nrf2 in ovarian cancer cells

Jia Zhou[1], Zhidong Qiu[1], Fang Zhou[2], Guo Xin[2], Ning Kong[3], Guangfu Lv[4], He Lin[1], Zhe Lin[1], Yangxin Fu[5], Yuchen Wang[1,*], Xiaowei Huang[6,*]

[1] *College of Pharmacy, Changchun University of Chinese Medicine, Changchun 130117, China*
[2] *Affiliated Hospital of Changchun University of Traditional Chinese Medicine, Changchun 130021, China*
[3] *College of Pharmacy, Jilin University, Changchun 130012, China*
[4] *Ginseng Science Research Institute, Changchun University of Chinese Medicine, Changchun 130117, China*
[5] *Department of Oncology, Faculty of Medicine and Dentistry, University of Alberta, Edmonton, AB T6G 2E1, Canada*
[6] *Northeast Asia Institute of Traditional Chinese Medicine, Changchun University of Chinese Medicine, Changchun 130117, China*

Article Info

Article history:

Received: January 10, 2024
Accepted: February 21, 2024
Published: March 31, 2024

Use your device to scan and read the article online

Abstract

Ovarian cancer is a prevalent malignancy in the female reproductive system, representing a significantly fatal and incurable tumor. Chelerythrine (CHE), a natural benzopyridine alkaloid, has demonstrated a broad spectrum of anticancer activities. Nevertheless, the ovarian cancer inhibitory impact of CHE remains unclear. In this study, we investigated the cytotoxic mechanism and potential targets of CHE on in vitro cultures of A2780 and SKOV3 cells derived from ovarian cancer. Additionally, in vivo experiments were conducted to confirm the suppressive impact of CHE on tumor growth in nude mice. The findings revealed that CHE impeded the growth of A2780 and SKOV3 cells in a concentration-time-dependent manner and significantly suppressed the development of tumors in nude mice. CHE elevated the level of oxidative stress in tumor cells, prompted cell cycle halt in the S phase, and increased their mitochondrial membrane potential. Western blotting results demonstrated that CHE could modulate the expression of proteins associated with apoptotic and ferroptosis processes in A2780 and SKOV3 cells. Nrf2 was verified to be an upstream key target mediating the inhibitory impact of CHE on ovarian cancer cells. In summary, CHE exerts its anti-cancer effects on ovarian cancer by modulating Nrf2, inhibiting cellular proliferation, and promoting apoptosis and ferroptosis.

Keywords: Chelerythrine, Ovarian cancer, Apoptosis, Ferroptosis, Nrf2.

1. Introduction

Ovarian cancer, a predominant gynecologic tumor originating from the ovary, uterus, and related tissues, represents the acknowledged 'king of gynecological cancers' with the highest mortality, lowest cure rate, and greatest recurrence rate among its counterparts [1, 2]. A survey conducted by the American Cancer Society forecasts nearly 20,000 fresh incidents of ovarian cancer are projected to occur in the United States in 2022, accompanied by over 12,000 fatalities [3]. Presently, clinical approaches to ovarian cancer treatment primarily involve tumor debulking surgery and adjuvant chemotherapy using platinum-based drugs [4]. However, owing to the intricate structure of ovarian tissue, subtle manifestations in the initial phases, and the absence of reliable screening techniques, the disease is often identified at advanced stages, leading to an increased recurrence rate and reduced survival rate over a 5-year period for advanced ovarian cancer [5]. Consequently, there is a pressing need to discover novel drugs and targets for enhancing the clinical management of ovarian cancer.

Chelerythrine (CHE), a benzylisoquinoline alkaloid sourced from *Papaveraceae* and *Rutaceae* [6], displays a wide range of advantageous effects, encompassing anti-inflammatory, antibacterial, and antiviral properties, making it a staple in agriculture and animal husbandry [7-9]. Moreover, numerous studies highlight CHE's promising efficacy against liver cancer, colorectal cancer, lung cancer, and glioblastoma [10-14]. Recent investigations underscore CHE's ability to induce oxidative stress across diverse cancer cell types. Liang et al. discovered that CHE triggers apoptosis in colorectal cancer cells by inducing cell cycle arrest and fostering the accumulation of reactive oxygen species (ROS) [11]. Similarly, He et al. observed an elevation in ROS levels within renal cell carcinoma (RCC) cells upon exposure to CHE, precipitating

* Corresponding author.
E-mail address: wangyc01@ccucm.edu.cn; huangxw@ccucm.edu.cn (Y. Wang, X. Huang).
Doi: http://dx.doi.org/10.14715/cmb/2024.70.3.26

endoplasmic reticulum stress and subsequent apoptosis [15]. Furthermore, research in zebrafish has unveiled that CHE's developmental toxicity hinges on its control of intracellular ROS levels, involving the inhibition of Nrf2 and the upregulation of recombinant Keap1, a specific target of Nrf2 [16].

The obtained results strongly indicate that CHE holds promise as an outstanding anti-tumor drug, with the heightened cytotoxicity likely associated with the provocation of oxidative stress. Nevertheless, the involvement of CHE in anti-ovarian research remains uncharted, and a deeper exploration into the underlying molecular mechanisms of its anti-tumor effects is imperative. This study aims to explore the influence of CHE on ovarian cancer cells, both within living organisms and in controlled laboratory conditions, with the overarching goal of elucidating its potential mechanism of action. The ultimate objective is to present novel therapeutic concepts and drugs aimed at addressing ovarian cancer clinically.

2. Materials and Methods

2.1. Cells

The source of the A2780 and SKOV3 cells was Procell Life Science and Technology Co., Ltd (Wuhan, China).

2.2. Animals

Twenty female nude mice of the BALB/c strain, acquired from Changchun Yisi Laboratory Animal Technology Co., LTD (SCXK (Ji) 2020-0002), with an age range of 4-6 weeks and a weight range of 16-18 g. Prior to the commencement of the experiment, a one-week adaptation period was provided for the animals. The ambient conditions were upheld at a constant temperature of 20-25°C, along with a relative humidity ranging between 40% and 60%. All procedures were conducted in strict accordance with the relevant management and ethical requirements for laboratory animals at Changchun University of Chinese Medicine. The animals were accommodated and operated upon with utmost care to ensure compliance with ethical standards.

2.3. Chemicals and reagents

CHE (purity>98%, B20052) was purchased from Yuanye Biotechnology Co., LTD (Shanghai, China). EdU-488 Cell Proliferation Assay Kit (#C0071S), Annexin V-FITC Kit (#C1052), Mitochondrial Membrane Potential Assay Kit (#C2006), and TUNEL Apoptosis Detection Kit (#C1089) were purchased from Beyotime Biology Technology Co., LTD (Shanghai, China). ROS Assay Kit (#CA1410), SOD Activity Detection Kit (#BC5165), MDA Content Detection Kit (#BC0025), GSH Content Detection Kit (#BC1175), Cell Iron Content Detection Kit (#BC5315) and TBHQ (#SB8960) were purchased from Solarbio Science and Technology Co., LTD (Shanghai, China). Apoptosis-related antibody (Bax, #50599; Bcl-2, #26593; cleaved-caspase3, #19677), ferroptosis-related antibody (Keap1, #10503; Nrf2, #16396; HO-1, #10701; GPX4, #30388) and β-actin (#20536) antibodies were purchased from Proteintech Biology Technology Co., LTD (Wuhan, China).

2.4. Cell viability assay

A2780 and SKOV3 cells were evenly inoculated into 96-well plates. After 24 hours, different concentrations of CHE (0, 2.5, 5.0, 7.5, 10.0, 15.0 and 20.0 μM) or TBHQ 10.0 μM+CHE were added to each group, and each group had five replicates. After 24, 48, and 72 h of incubation, MTT assay detects the cell viabilities. The optical density (OD) at 570nm was assessed with a multifunctional enzyme marker.

2.5. Colony formation assay

A2780 and SKOV3 cells were evenly inoculated into 6-well plates, with 100 cells per well. Then the cells were cultured under conditions of 37°C and 5% CO_2 for 24 hours. CHE0, 5, 10, and 15μM were added to each well, respectively. Following 2 weeks of cultivation, the cells were treated with 4% paraformaldehyde for fixation, subjected to staining using a crystal violet solution, photographed, and the colonies were subsequently counted.

2.6. Edu staining assay

In the 6-well plate, an appropriate number of A2780 and SKOV3 cells were cultured. CHE0, 5, 10, and 15 μM were added to each group of cells at a temperature of 37°C and in an environment with 5% CO_2 for 24 hours. The preheated Edu working solution at 37°C was introduced into each well. After 2 hours of incubating, wash and fix the wells, and the Click reaction solution was added and incubated for 30 minutes, followed by staining of cell nuclei with Hoechst 33342. Cell proliferation was observed and counted under a fluorescence microscope.

2.7. Flow cytometer assay

Each group of cells was with 0, 5, 10, and 15 μM of CHE or 0, 15 μM of CHE and 10 μM TBHQ+15 μM CHE for 24 hours. Post-treatment, the cells were trypsinized (sans calcium and magnesium ions) and a collection of 100,000 cells per group was gathered. After washing, the cells were resuspended in the binding buffer. Changes in the cell cycle, apoptosis, and mitochondrial membrane potential (MMP) post-drug treatment were assessed respectively.

2.8. ROS, oxidative stress, and ferroptosis levels

Intracellular ROS levels in cells were determined by in situ probe loading. Each group of cells was with 0, 5, 10, and 15 μM of CHE or 0, 15 μM of CHE and 10 μM TBHQ+15 μM CHE for 24 hours. Then, a diluted DCFH-DA probe solution was substituted, and incubation of the cells persisted for 20 minutes at 37°C. Following incubation, the cells were washed and ROS production was visualized and photographed using a fluorescence microscope set to emit light at 488 nm. For the biochemical assays, cells were treated for 24 hours with either 0 and 15μM CHE or a combination of 0, 15 μM CHE, and 10 μM TBHQ+15 μM CHE. Post-treatment, the levels of SOD, MDA, GSH, and Fe^{2+} in the cells were quantified following the manufacturer's guidelines.

2.9. TUNEL assay

Cells were subjected to treatments with 0, 5, 10, and 15 μM CHE. After 24 hours, cells were rinsed with PBS, fixed for 30 minutes, and permeabilized with 0.3% Triton X-100. The TUNEL assay solution was introduced to each well, and the cells were allowed to incubate at 37°C in the dark for 60 minutes. After rinsing, the slides were blocked with anti-fluorescence quenching mounting solution, and

the apoptosis of cells was examined using a fluorescence microscope.

2.10. Xenograft studies in nude mice

The suspension of SKOV3-luc cells in logarithmic growth phase (1×10^7/mL) was inoculated subcutaneously into the left anterior groin of nude mice, 0.2 mL for each mouse. Successful establishment of the tumor model was confirmed by the measurement of an average tumor volume of 100 mm^3 at the site of injection. The nude mice that were successfully modeled underwent random allocation into the following groups: control group, positive drug cisplatin group (DDP, 3 mg/kg), CHE high dose group (10 mg/kg), and CHE low dose group (5 mg/kg), with 5 mice per group. The control group was administered daily intraperitoneal injections of 0.2 mL of 0.9% saline solution, while the DDP group was administered cisplatin (3 mg/kg) intraperitoneally every two days. The CHE groups were treated with their respective doses daily for 28 days. Tumor dimensions were quantified every seven days using a small animal imaging system and a vernier caliper, facilitating the calculation of tumor volumes. At the conclusion of the 28-day period, tumor tissues were harvested from the mice for further analyses.

2.11. Western blot assay

The total protein extract concentration was determined using the BCA Protein Concentration Assay kit. SDS-PAGE gels of varying concentrations were prepared using a one-step rapid gel preparation kit. The electrophoresed proteins were subsequently transferred onto PVDF membranes and subjected to blocking with 7% skim milk powder. Following this, the respective primary antibody was applied and allowed to incubate overnight in 4°C refrigerator. After TBST thorough washing, the secondary antibody was introduced and incubated for 2 hours. The ECL luminescent solution was employed, and a multifunctional chemiluminescence imager was utilized for image capture. Subsequent analysis of band intensity was performed using Image J software, facilitating accurate quantification of the observed protein bands. β-actin was used as an internal reference.

2.12. Statistical analysis

Statistical analysis of experimental data was conducted using GraphPad Prism8.0 software (La Jolla, CA, USA). All experimental results were found to conform to a normal distribution and have equal variances. The data were presented as mean ± standard deviation. Multiple comparisons were conducted using one-way analysis of variance (ANOVA) with Tukey's post hoc test. Statistical significance was defined at a level of $P < 0.05$.

3. Results

3.1. CHE inhibits proliferation of A2780 and SKOV3 cells

A2780 and SKOV3, two ovarian cancer cell lines, were chosen to assess the antitumor capability of CHE. The structural composition of CHE is shown in Figure 1A. CHE was determined by MTT method to detect different concentrations (0, 2.5, 5.0, 7.5, 10.0, 15.0, 20.0 μM) cell proliferation rate after treatment. The results showed that CHE inhibited the cell viability of A2780 and SKOV3 cells in a dose and time-dependent manner (Figure 1B), with IC50 values of 12.84 μM and 7.98 μM. The morphological changes of the cells after CHE treatment were observed by microscope: after CHE treatment, the cell adhesion became worse and the cell morphology shrunk compared with the control group (Figure 1C). The results of the colony formation assay showed that CHE could reduce the colony formation of the cells (Figure 1D). The findings from Edu staining demonstrated a decrease in the number of Edu-positive cells as the concentration of CHE increased (Figure 1E). The outcomes of cell cycle analysis indicated that CHE significantly increased the distribution of A2780 and SKOV3 cells in the S phase, indicating that CHE arrested cells in the DNA division phase (Figure 1F, G). These findings indicated that, in *vitro*, CHE could effectively hinder the proliferation of ovarian cancer cells A2780 and SKOV3.

3.2. CHE induces oxidative stress and mitochondrial depolarization in A2780 and SKOV3 cells

The outcomes displayed a notable increase in the fluorescence intensity within the group treated with CHE when compared to the control group. This increase suggests a heightened level of intracellular ROS (Figure 2A). Concurrently, in comparison with the control group, the CHE administration group exhibited a noteworthy reduction in the level of superoxide dismutase (SOD) and a marked increase in malondialdehyde (MDA) levels (Figure 2B). These alterations signify a state of oxidative

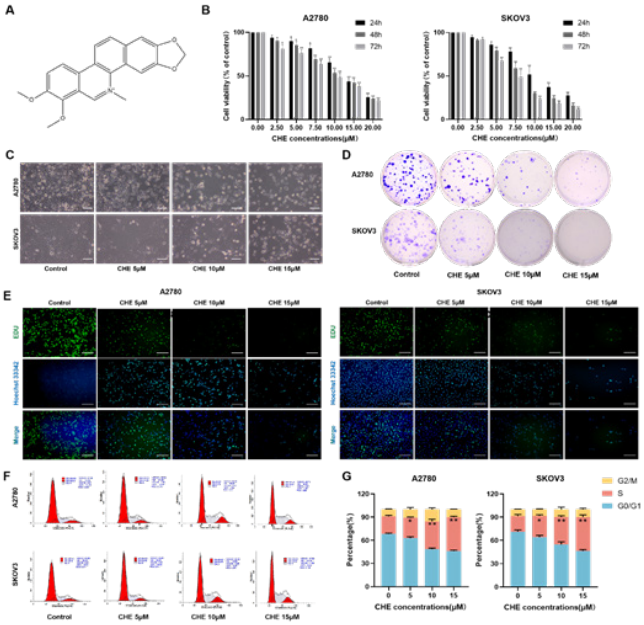

Fig. 1. CHE inhibits cell proliferation in ovarian cancer cells. (A) Chemical structure of Chelerythrine. (B) Cell viability after treating 0, 2.5, 5.0, 7.5, 10.0, 15.0, 20.0 μM CHE for 24, 48, 72 h. (C) Morphological changes of A2780 and SKOV3 cells treated with CHE after 24 h. (D) The presented images depict colony formation, with the colonies subsequently subjected to staining using crystal violet staining solution. (E) Edu staining results of A2780 and SKOV3 cells after CHE treatment showed that EdU-488(green) represented the number of cell proliferation and Hoechst 33342(blue) represented the total number of cells. (F, G) Cell cycle distribution (F) and the percentage (G) in various phases of the A2780 and SKOV3 cells treated with CHE (5, 10 and 15 μM) for 24 h via Flow cytometry. The statistical results are expressed as the mean ± SD, n = 3, * $P < 0.05$, ** $P < 0.01$ vs. control group.

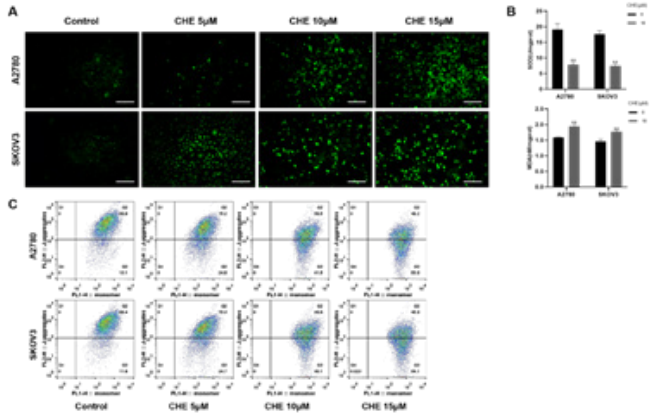

Fig. 2. CHE triggers oxidative stress and disrupts MMP in ovarian cancer cells. (A) The fluorescent probe DCFH-DA was employed to measure intracellular ROS levels in A2780 and SKOV3 cells following 24 hours of CHE treatment; green dots in the graph indicate positive fluorescence for ROS. (B) The relative levels of SOD and MDA in each group. (C) MMP in A2780 and SKOV3 cells after 24 h of CHE treatment. Scale bar: 100 μm. The statistical results are expressed as the mean ± SD, n = 3, * $P < 0.05$, ** $P < 0.01$ vs. control group.

stress within the cells following CHE administration. To further investigate the impact of CHE on cellular physiology, flow cytometry was employed to assess changes in MMP. The results demonstrated that the groups subjected to CHE treatment exhibited a decrease in MMP, signifying mitochondrial depolarization (Figure 2C).

3.3. CHE-induced apoptosis and cycle arrest in A2780 and SKOV3 cells

The findings from flow cytometry demonstrated a progressive elevation in the apoptosis rate corresponding to the escalating concentration of CHE administration when compared to the control group (Figure 3A). The outcomes of TUNEL staining illustrated a notable rise in the count of TUNEL-positive cells after CHE treatment (Figure 3B). The Western blot results indicated that in comparison to the control group, the CHE administration group exhibited a substantial increase in the expression levels of Bax and cleaved-caspase3, along with a significant decrease in the expression level of Bcl-2 (Figure 3C-F). These results provide evidence supporting the capacity of CHE to trigger apoptosis in A2780 and SKOV3 cells in an *in vitro* setting.

3.4. CHE-induced ferroptosis in A2780 and SKOV3 cells

In comparison to the control group, the group treated with CHE exhibited a noteworthy decrease in GSH levels (Figure 4A) and a marked accumulation of Fe^{2+} (Figure 4B). Western blot analysis of ferroptosis-related protein expression in the cells revealed a significant elevation in Keap1 levels, accompanied by a substantial reduction in Nrf2, HO-1, and GPX4 protein levels following treatment with CHE (Figure 4C-G). These results suggested that CHE has the capability to trigger ferroptosis in A2780 and SKOV3 cells in an *in vitro* setting.

3.5. CHE inhibits the growth of SKOV3-luc xenografts in nude mice

The experimental results demonstrated that in comparison to the control group, the positive drug group, the high-dose CHE group, and the low-dose CHE group exhibited a comparatively reduced tumor growth rate (Figure 5A). After 28 days of drug administration, tumor volumes were significantly smaller in the positive drug group, the CHE high-dose group, and the CHE low-dose group than in the control group (Figure 5B). The results indicated that there was no notable distinction in tumor weight between the positive drug group and the high-dose CHE group. However, the tumor weights of both the positive drug group, the high-dose CHE group, and the low-dose CHE group were significantly lower than those of the control group (Figure 5C-D). The Nrf2 protein expression in the cells was assessed through Western blot analysis, revealing that both DDP and CHE treatments led to a decrease in the expression level of Nrf2 protein (Figure 5E). These findings imply that CHE has the potential to hinder *in vivo* tumor

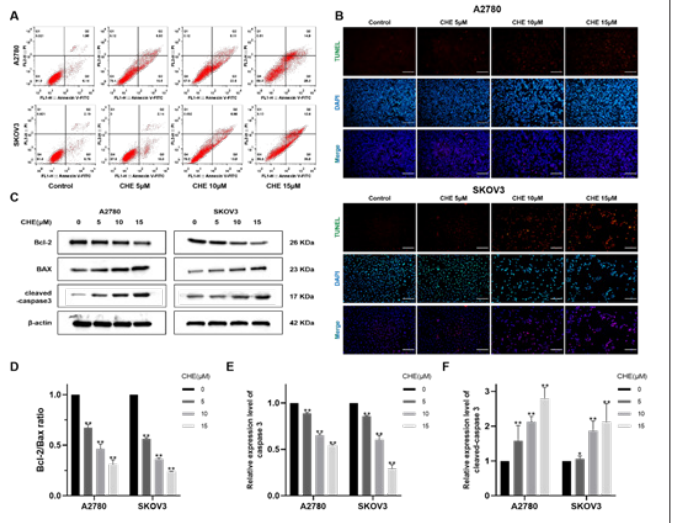

Fig. 3. CHE-induced apoptosis in ovarian cancer cells. (A) Flow cytometry dot pot of cells after treatment with CHE (5, 10 and 15 μM) for 24 h. (B) TUNEL staining assay was used to detect apoptosis, where apoptotic cells were depicted by TUNEL (red), while nuclei were visualized using DAPI (blue). (C-F) Western blot analysis was employed to assess the protein expression levels of apoptosis-related proteins in A2780 and SKOV3 cells following treatment with CHE at concentrations of 5, 10, and 15 μM for a duration of 24 hours. Scale bar: 100 μm. The statistical results are expressed as the mean ± SD, n = 3, * $P < 0.05$, ** $P < 0.01$ vs. control group.

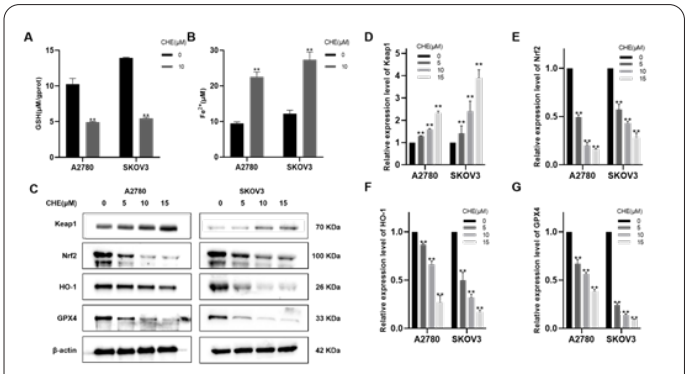

Fig. 4. CHE promotes ferroptosis in ovarian cancer cells. (A) The relative levels of GSH. (B) The relative levels of Fe^{2+}. (C-G) The impact of CHE on ferroptosis-related proteins in cells was assessed through a Western blot assay, with normalization of all protein levels to β-actin. The statistical results are expressed as the mean ± SD, n = 3, ** $P < 0.01$ vs. control group.

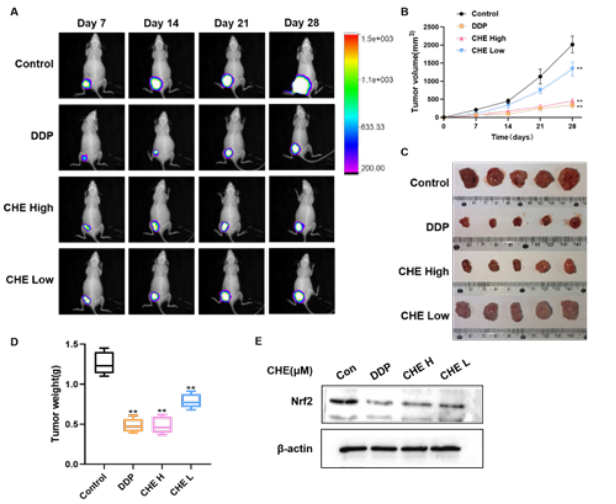

Fig. 5. CHE inhibited the tumor growth of SKOV3-luc in nude mice. (A) Representative bioluminescence images of each group. (B) Tumor volume growth trajectory. (C) Tumor anatomy of SKOV3-luc subcutaneous tumor-bearing mice. (D) Average final tumor weights of each group. CHE inhibits cell proliferation in ovarian cancer cells. The statistical results are expressed as the mean ± SD, n = 5, ** $P <$ 0.01 vs. control group.

growth, and the underlying mechanism may be associated with the suppression of Nrf2 protein expression.

3.6. CHE triggers apoptosis and ferroptosis by regulating Nrf2 in A2780 and SKOV3 cells

Recent investigations have elucidated the pivotal involvement of Nrf2 in the intricate processes of tumor cell proliferation, apoptosis, and ferroptosis (28,29). Synthesizing these insights with the findings from prior studies, we posit a hypothesis that CHE may exert its influence on apoptosis and ferroptosis in cells through the regulatory adjustment of Nrf2. Moreover, in this study, tertiary butylhydroquinone (TBHQ), recognized as an activator of the Nrf2 pathway, was chosen for co-treatment with CHE to selectively trigger the Nrf2 pathway in ovarian cancer cells (30). The MTT assay results indicated a notable reduction in the suppressive impact of CHE on cell proliferation following co-treatment with TBHQ (Figure 6A). The assessment of oxidative stress using the DCFH-DA probe revealed that the TBHQ+CHE group exhibited a significantly lower level of ROS compared to the CHE group (Figure 6B). Additionally, the TBHQ+CHE group demonstrated a markedly elevated intracellular SOD level (Figure 6C) and a significantly reduced MDA level (Figure 6D) in comparison to the CHE group. The flow cytometry results revealed a notable decrease in the quantity of apoptotic cells in the TBHQ+CHE group as opposed to the CHE group, indicating that TBHQ has the potential to counteract the pro-apoptotic effects of CHE (Figure 6E). Furthermore, assessments of ferroptosis-related indicators demonstrated that, in comparison to the CHE group, the simultaneous administration of TBHQ and CHE resulted in an elevation of intracellular GSH levels and a reduction in Fe^{2+} levels. These findings indicate that the induction of the Nrf2 signaling pathway by TBHQ could, to some extent, mitigate the impact of CHE (Figure 6G-H). Following this, we performed Western blot analysis to assess the protein expression levels of Keap1, Nrf2, HO-1, and GPX4. The findings indicated a decrease in Keap1 expression and an elevation in the expression of Nrf2, HO-1, and GPX4 in the TBHQ+CHE group compared to the CHE group (Figure 6F). These results imply that the suppression of Nrf2 by CHE may play a role in enhancing ferroptosis in ovarian cancer cells.

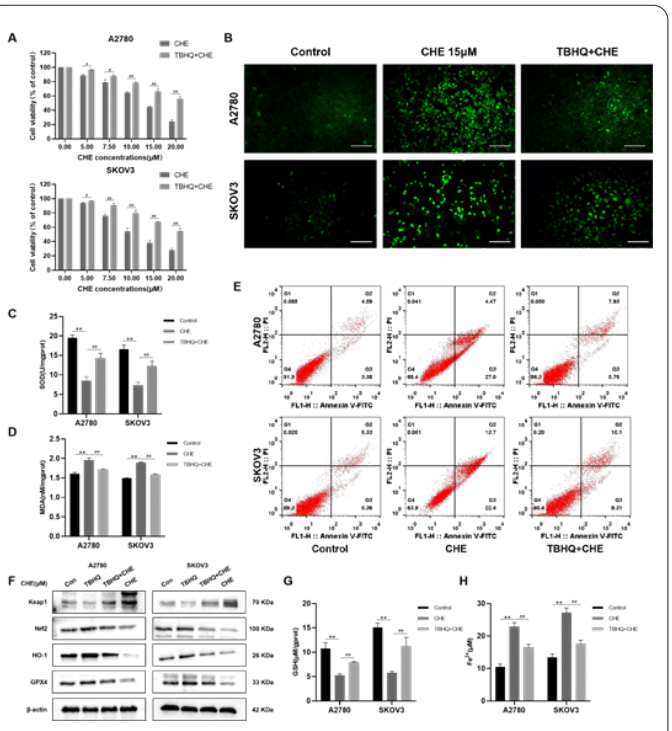

Fig. 5. CHE triggers apoptosis and ferroptosis by regulating Nrf2. (A) Cell viability was assessed through MTT assay in cells following exposure to the combination of TBHQ and CHE. (B) ROS levels were measured utilizing the fluorescence probe DCFH-DA through immunofluorescence in cells after simultaneous treatment with TBHQ. Positive fluorescence for ROS is depicted by the green dots in the figures. (C, D) The relative levels of SOD and MDA. (E) Cell apoptosis was quantified using flow cytometry subsequent to co-treatment with TBHQ. (F) The levels of Nrf2, HO-1, and GPX4 expression were identified in A2780 and SKOV3 cells subjected to TBHQ treatment. All protein levels were standardized to β-actin. (G, H) The relative levels of GSH and Fe^{2+}. Scale bar: 100 μm. The statistical results are expressed as the mean ± SD, n = 3, * $p < 0.05$, ** $P < 0.01$ vs. control group; # $P < 0.05$, ## $P < 0.01$ vs. TBHQ+CHE.

4. Discussion

CHE, a compound derived from botanical sources including *Chelidonium majus* L., *Macleaya cordata* R. Br., *Zanthoxylum nitidum* DC., and *Zanthoxylum* bungeanum, comprises alkaloids extracted from natural medicinal plants like Maxim. The chemical nomenclature designates it as 1,2-dimethoxy-12-methyl-[1,3]benzodioxolo[5,6-C]phenanthridin-12-ium, with a molecular formula of $C_{21}H_{18}NO_4^+$ (20). In 1990, Herbert J.M. proposed that CHE served as a robust and specific inhibitor of protein kinase C (PKC). It stood out as the most effective and selective inhibitor of PKC, targeting the substrate-binding sites of PKC [20]. As a result, it gained extensive utilization in both medical and scientific research. Several studies have indicated that CHE functions as a BH3 mimic, effectively substituting the BH3 protein in BclXL to bind GST-BclXL. This action allows it to overcome the upstream anti-apoptotic barrier in transformed cells, interrupt the association between Bcl-2 and Bax, and thereby facilitate apoptosis [21]. Furthermore, researches has demonstrated that CHE can

prompt rapid apoptosis of cells, and its mechanism may be associated with the elevation of ROS, substantial H2O2 production, and the consumption of cellular antioxidants [22]. However, the involvement and underlying mechanism of CHE in ovarian cancer are still inadequately elucidated. Our study aims to systematically investigate the impact of CHE on ovarian cancer both *in vitro* and *in vivo*. In our research, the results indicated that CHE demonstrated noteworthy anti-tumor efficacy in ovarian cancer cells, and it effectively hindered tumor growth in nude mice. Mechanistically, CHE inhibited Nrf2 expression, resulting in elevated levels of ROS. This, in turn, instigated apoptosis and ferroptosis.

As a by-product of aerobic respiration, ROS plays a pivotal role in regulating tissue homeostasis, cell signaling, differentiation, and survival [23]. Simultaneously, in the initiation and progression of tumors, ROS plays a role in regulating the tumor microenvironment, affecting stromal cells to contribute metabolic support, vascularization, and immune responses to tumors [24]. Studies have demonstrated that the effectiveness of diverse anticancer medications is primarily attained by elevating intracellular ROS levels. The drug-induced rise in ROS can result in oxidative damage to DNA, proteins, and lipids, thereby initiating cell death and promoting apoptosis [25].

Apoptosis is a gene-encoded cell death program, which can selectively initiate self-death in cells, thereby preserving a crucial equilibrium between cell survival and death. It occupies a central position in both physiological and pathological processes within the human body [26]. The onset of cancer frequently coincides with dysregulation in the apoptotic pathway. On the one hand, apoptosis deficiency offers oxidative stress protection to tumors; on the other hand, the self-destruction mechanism of DNA-deficient cells is inhibited, allowing the survival of genetically unstable cells and consequently promoting tumorigenesis [27, 28]. ROS holds significant import in the induction of apoptosis and serves as the primary molecular objective for numerous anticancer therapeutics. High levels of ROS can result in mitochondrial dysfunction, release cytochrome C and other proteins in mitochondria, and activate caspases [29]. Caspases, a subset of proteases specifically reactive towards cysteine, assume a pivotal function in effectuating apoptosis. Through their activation, ROS effectively instigates the commencement of the apoptotic cascade, leading to cell death. The experimental findings from our study demonstrate mitochondrial depolarization in cells subsequent to CHE treatment, coinciding with the onset of early apoptosis. Tunel staining revealed a notable increase in positively stained cells. Additionally, we assessed the levels of key apoptosis regulatory proteins—Bax, Bcl-2, and cleaved-caspase3. The results indicate a significant elevation in both the Bax/Bcl-2 ratio and the expression of cleaved-caspase3 within ovarian cancer cells post-CHE treatment, providing further evidence for the induction of mitochondria-dependent apoptosis [30].

Nrf2, belonging to the cap'n'collar (CNC) family and serving as a crucial regulator of ROS, functions as an intracellular oxidative stress sensor, playing a pivotal role in cellular resistance to oxidative stress [24, 31]. Additionally, it exerts a positive influence on various pathways, including apoptosis, mitochondrial function, DNA damage repair, and ferroptosis [32, 33]. In normal cells, a comprehensive anti-oxidative stress system is present, where Nrf2 and its signaling protein Keap1 form a cytoplasmic complex susceptible to targeted degradation.

Upon the onset of oxidative challenge, increased ROS levels trigger the phosphorylation of Nrf2, facilitating its translocation into the nucleus. There, it establishes a transcriptional activation complex alongside Maf proteins, engaging antioxidant response elements (ARE) and activating a cascade of downstream antioxidant factors [34, 35]. However, in the context of cancer, Nrf2 assumes a deleterious role. Induction of Nrf2 in cancer cells is facilitated by various pathways, such as Keap1 functional mutation, K-Ras signaling, and phosphorylation of Keap1 residues by protein kinase C (PKC). This activation enhances the antioxidant capacity, drug resistance, invasion, and metastasis of tumor cells [31]. Studies have consistently reported a substantial up-regulation of Nrf2 expression across diverse malignancies, encompassing ovarian cancer, head and neck cancer, lung cancer, and breast cancer [36-39]. Consequently, the inhibition of Nrf2 activity holds substantial potential in cancer therapy. Luteolin increases the responsiveness of lung cancer cells to drugs by promoting the degradation of Nrf2 mRNA [40]. Moreover, luteolin demonstrates the capability to diminish the expression of Nrf2 protein, promote the proliferation of liver and intestinal tumors, and trigger apoptosis in mice [41]. In antitumor investigations of dihydrotanshinone I (DHT), it has been observed that DHT activates oxidative stress by mediating the ubiquitination-induced degradation of Nrf2. As a result, there is a suppression of Nrf2 and p62 expression, subsequently prompting apoptosis and cell cycle arrest. Additionally, DHT exhibits tumor growth-delaying properties in nude mice [42].

In our study, we initially assessed the protein expression related to the Nrf2 signaling pathway within cells. Our findings demonstrated that CHE augmented the expression of the Nrf2 signaling protein Keap1, inhibited Nrf2, and diminished the levels of downstream antioxidant proteins like HO-1 and the ferroptosis-associated protein GPX4. A decrease in Nrf2 expression was also observed in tumor tissues of nude mice. To delve deeper into the antitumor mechanism of CHE, we co-treated cells with the Nrf2 activator TBHQ to investigate whether CHE's antitumor effect was mediated through Nrf2 inhibition. The results demonstrated that co-treatment with TBHQ led to a relative increase in Nrf2 protein expression. This partially countered CHE's suppressive impact on the proliferation of ovarian cancer cells and reversed the apoptosis induced by CHE. These experimental outcomes aligned with our hypothesis.

Intriguingly, besides triggering apoptosis in ovarian cancer cells, our study revealed the involvement of ferroptosis. Ferroptosis, a recently identified form of oxidative and non-apoptotic programmed cell death, is characterized by damage to iron-dependent lipid peroxides and a reduction in the activity of the lipid-repair enzyme GPX4. This process is marked by increased accumulation of ROS, iron overload, and lipid peroxides [6, 7]. Growing evidence suggests that modulating ferroptosis can impede tumor proliferation and migration. For instance, Xiang et al. demonstrated that the natural product Erianin induces ferroptosis in bladder cancer cells RT4 and KU-19-19 by promoting ROS accumulation and depleting GSH. The induction of ferroptosis by Erianin was further enhanced after inhibiting Nrf2 expression using siRNA [37]. Simi-

larly, Chen et al. observed that NSCLC cells treated with ShtIX exhibited increased Fe^{2+} content, lipid peroxidation accumulation, and decreased GPX4 expression. Concurrently, the protein expression of Nrf2 and HO-1 decreased [38]. In line with these findings, our study demonstrated that CHE elevates ROS levels in cells by inhibiting Nrf2 expression, depletes GSH, induces iron accumulation, reduces GPX4 protein expression, and ultimately triggers ferroptosis in ovarian cancer cells.

5. Conclusions

In conclusion, our study demonstrated the inhibitory effect of CHE on the proliferation of ovarian cancer cell lines A2780 and SKOV3 *in vitro*. Subsequently, a xenograft tumor model was established in nude mice to verify the efficacy of the drug *in vivo*. CHE was found to induce apoptosis and ferroptosis in A2780 and SKOV3 cells by flow cytometry, fluorescence staining and Western Blot analysis, with Nrf2 identified as its primary target.

These findings not only enhance our comprehension of the mechanism responsible for the anti-tumor properties of CHE but also provide strong experimental validation for its potential application in the treatment of ovarian cancer.

Conflicts of interest

The authors declare no conflict of interest.

Institutional review board statement

The handling of animals was performed with the consent of protocols approved by the Experimental Animal Ethics Committee of Changchun University of Traditional Chinese Medicine (Approval Number: 2020231).

Informed consent statement

Not applicable.

Data availability statement

All data are available in this publication and in the Supplementary Materials.

Author contributions

Conceptualization, X.H. and Y.W.; methodology, G.L., H.L. and Y.F.; investigation, J.Z.; resources, Z.L., X.H. and G.X.; writing—original draft preparation, J.Z.; writing—review and editing, Z.Q and Y.W.; supervision, F.Z. and N.K.; project administration, J.Z. and Y.W.; funding acquisition, X.H. and G.X. All authors have read and agreed to the published version of the manuscript.

Funding

This research was funded by the Jilin Province Science and Technology Development Plan Project (Grant Number: 20210402034GH); the Jilin Provincial Development and Reform Commission (Grant Number: 2021C011); and the Jilin Province Traditional Chinese Medicine Science and Technology Funding Project (Grant Number: 2023041); Research Project of Chinese Association of Ethnic Medicine (Grant Number: 2023ZY147-36).

References

1. Hennessy BT, Coleman RL, Markman M (2009) Ovarian cancer. Lancet 374:1371-1382. doi: 10.1016/S0140-6736(09)61338-6
2. Mize BK, Salvi A, Ren Y, Burdette JE, Fuchs JR (2023) Discovery and development of botanical natural products and their analogues as therapeutics for ovarian cancer. Nat Prod Rep 40:1250-1270. doi: 10.1039/d2np00091a
3. Siegel RL, Miller KD, Fuchs HE, Jemal A (2022) Cancer statistics, 2022. Ca Cancer J Clin 72:7-33. doi: 10.3322/caac.21708
4. Kumar S, Raina M, Tankay K, Ingle GM (2023) Patient-derived organoids in ovarian cancer: Current research and its clinical relevance. Biochem Pharmacol 213:115589. doi: 10.1016/j.bcp.2023.115589
5. Lheureux S, Braunstein M, Oza AM (2019) Epithelial ovarian cancer: Evolution of management in the era of precision medicine. Ca Cancer J Clin 69:280-304. doi: 10.3322/caac.21559
6. Lee JY, Kim WK, Bae KH, Lee SC, Lee EW (2021) Lipid Metabolism and Ferroptosis. Biology (Basel) 10:184. doi: 10.3390/biology10030184
7. Bebber CM, Muller F, Prieto CL, Weber J, von Karstedt S (2020) Ferroptosis in Cancer Cell Biology. Cancers (Basel) 12:164. doi: 10.3390/cancers12010164
8. Peng F, Liao M, Qin R, Zhu S, Peng C, Fu L et al (2022) Regulated cell death (RCD) in cancer: key pathways and targeted therapies. Signal Transduct Target Ther 7:286. doi: 10.1038/s41392-022-01110-y
9. Li J, Yi X, Liu L, Wang X, Ai J (2023) Advances in tumor nanotechnology: theragnostic implications in tumors via targeting regulated cell death. Apoptosis 28:1198-1215. doi: 10.1007/s10495-023-01851-3
10. Zhao L, Zhou X, Xie F, Zhang L, Yan H, Huang J et al (2022) Ferroptosis in cancer and cancer immunotherapy. Cancer Commun (Lond) 42:88-116. doi: 10.1002/cac2.12250
11. Hassannia B, Vandenabeele P, Vanden BT (2019) Targeting Ferroptosis to Iron Out Cancer. Cancer Cell 35:830-849. doi: 10.1016/j.ccell.2019.04.002
12. Chen X, Kang R, Kroemer G, Tang D (2021) Broadening horizons: the role of ferroptosis in cancer. Nat Rev Clin Oncol 18:280-296. doi: 10.1038/s41571-020-00462-0
13. Cao J, Zheng Y, Liu T, Liu J, Liu J, Wang J et al (2022) Fluorescence, Absorption, Chromatography and Structural Transformation of Chelerythrine and Ethoxychelerythrine in Protic Solvents: A Comparative Study. Molecules 27:4693. doi: 10.3390/molecules27154693
14. Cao L, Liang Y, Zhao F, Zhao X, Chen Z (2016) Chelerythrine and Fe3O4 Loaded Multi-Walled Carbon Nanotubes for Targeted Cancer Therapy. J Biomed Nanotechnol 12:1312-1322. doi: 10.1166/jbn.2016.2280
15. Liang D, Liu L, Zheng Q, Zhao M, Zhang G, Tang S et al (2023) Chelerythrine chloride inhibits the progression of colorectal cancer by targeting cancer-associated fibroblasts through intervention with WNT10B/beta-catenin and TGFbeta2/Smad2/3 axis. Phytother Res 37:4674-4689. doi: 10.1002/ptr.7934
16. Tang ZH, Cao WX, Wang ZY, Lu JH, Liu B, Chen X et al (2017) Induction of reactive oxygen species-stimulated distinctive autophagy by chelerythrine in non-small cell lung cancer cells. Redox Biol 12:367-376. doi: 10.1016/j.redox.2017.03.009
17. Adinolfi S, Patinen T, Jawahar DA, Pitkanen S, Harkonen J, Kansanen E et al (2023) The KEAP1-NRF2 pathway: Targets for therapy and role in cancer. Redox Biol 63:102726. doi: 10.1016/j.redox.2023.102726
18. Tian Y, Liu H, Wang M, Wang R, Yi G, Zhang M et al (2022) Role of STAT3 and NRF2 in Tumors: Potential Targets for Antitumor Therapy. Molecules 27:8768. doi: 10.3390/molecules27248768
19. Shih AY, Li P, Murphy TH (2005) A small-molecule-inducible Nrf2-mediated antioxidant response provides effective prophylaxis against cerebral ischemia in vivo. J Neurosci 25:10321-10335. doi: 10.1523/JNEUROSCI.4014-05.2005

20. Herbert JM, Augereau JM, Gleye J, Maffrand JP (1990) Chelerythrine is a potent and specific inhibitor of protein kinase C. Biochem Biophys Res Commun 172:993-999. doi: 10.1016/0006-291x(90)91544-3
21. Chan SL, Lee MC, Tan KO, Yang LK, Lee AS, Flotow H et al (2003) Identification of chelerythrine as an inhibitor of BclXL function. J Biol Chem 278:20453-20456. doi: 10.1074/jbc.C300138200
22. Matkar SS, Wrischnik LA, Hellmann-Blumberg U (2008) Production of hydrogen peroxide and redox cycling can explain how sanguinarine and chelerythrine induce rapid apoptosis. Arch Biochem Biophys 477:43-52. doi: 10.1016/j.abb.2008.05.019
23. Harris IS, DeNicola GM (2020) The Complex Interplay between Antioxidants and ROS in Cancer. Trends Cell Biol 30:440-451. doi: 10.1016/j.tcb.2020.03.002
24. Cheung EC, Vousden KH (2022) The role of ROS in tumour development and progression. Nat Rev Cancer 22:280-297. doi: 10.1038/s41568-021-00435-0
25. Eccleston A (2023) A ROS-mediated resistance pathway to anticancer drugs. Nat Rev Drug Discov 22:534. doi: 10.1038/d41573-023-00094-w
26. Campbell KJ, Tait S (2018) Targeting BCL-2 regulated apoptosis in cancer. Open Biol 8:180002. doi: 10.1098/rsob.180002
27. Ionov Y, Yamamoto H, Krajewski S, Reed JC, Perucho M (2000) Mutational inactivation of the proapoptotic gene BAX confers selective advantage during tumor clonal evolution. Proc Natl Acad Sci U S A 97:10872-10877. doi: 10.1073/pnas.190210897
28. International BR (2020) Retracted: Apoptosis and Molecular Targeting Therapy in Cancer. Biomed Res Int 2020:2451249. doi: 10.1155/2020/2451249
29. Ren Y, Wang R, Weng S, Xu H, Zhang Y, Chen S et al (2023) Multifaceted role of redox pattern in the tumor immune microenvironment regarding autophagy and apoptosis. Mol Cancer 22:130. doi: 10.1186/s12943-023-01831-w
30. Green DR, Kroemer G (2004) The pathophysiology of mitochondrial cell death. Science 305:626-629. doi: 10.1126/science.1099320
31. Lillo-Moya J, Rojas-Sole C, Munoz-Salamanca D, Panieri E, Saso L, Rodrigo R (2021) Targeting Ferroptosis against Ischemia/Reperfusion Cardiac Injury. Antioxidants (Basel) 10:667. doi: 10.3390/antiox10050667
32. Yan N, Zhang J (2019) Iron Metabolism, Ferroptosis, and the Links With Alzheimer's Disease. Front Neurosci 13:1443. doi: 10.3389/fnins.2019.01443
33. Li L, Qiu C, Hou M, Wang X, Huang C, Zou J et al (2021) Ferroptosis in Ovarian Cancer: A Novel Therapeutic Strategy. Front Oncol 11:665945. doi: 10.3389/fonc.2021.665945
34. Kitamura H, Motohashi H (2018) NRF2 addiction in cancer cells. Cancer Sci 109:900-911. doi: 10.1111/cas.13537
35. Wang R, Liang L, Matsumoto M, Iwata K, Umemura A, He F (2023) Reactive Oxygen Species and NRF2 Signaling, Friends or Foes in Cancer? Biomolecules 13:353. doi: 10.3390/biom13020353
36. Bano I, Horky P, Abbas SQ, Majid M, Bilal A, Ali F et al (2022) Ferroptosis: A New Road towards Cancer Management. Molecules 27:2129. doi: 10.3390/molecules27072129
37. Xiang Y, Chen X, Wang W, Zhai L, Sun X, Feng J et al (2021) Natural Product Erianin Inhibits Bladder Cancer Cell Growth by Inducing Ferroptosis via NRF2 Inactivation. Front Pharmacol 12:775506. doi: 10.3389/fphar.2021.775506
38. Chen J, Zhou S, Zhang X, Zhao H (2022) S-3'-hydroxy-7', 2', 4'-trimethoxyisoxane, a novel ferroptosis inducer, promotes NSCLC cell death through inhibiting Nrf2/HO-1 signaling pathway. Front Pharmacol 13:973611. doi: 10.3389/fphar.2022.973611
39. Sajadimajd S, Khazaei M (2018) Oxidative Stress and Cancer: The Role of Nrf2. Curr Cancer Drug Targets 18:538-557. doi: 10.2174/1568009617666171002144228
40. Tang X, Wang H, Fan L, Wu X, Xin A, Ren H et al (2011) Luteolin inhibits Nrf2 leading to negative regulation of the Nrf2/ARE pathway and sensitization of human lung carcinoma A549 cells to therapeutic drugs. Free Radic Biol Med 50:1599-1609. doi: 10.1016/j.freeradbiomed.2011.03.008
41. Chian S, Thapa R, Chi Z, Wang XJ, Tang X (2014) Luteolin inhibits the Nrf2 signaling pathway and tumor growth in vivo. Biochem Biophys Res Commun 447:602-608. doi: 10.1016/j.bbrc.2014.04.039
42. Sun C, Han B, Zhai Y, Zhao H, Li X, Qian J et al (2022) Dihydrotanshinone I inhibits ovarian tumor growth by activating oxidative stress through Keap1-mediated Nrf2 ubiquitination degradation. Free Radic Biol Med 180:220-235. doi: 10.1016/j.freeradbiomed.2022.01.015